DOI: 10.18462/iir.icr.2023.0173

# Compressed liquid density and speed of sound measurements and correlation of the binary mixture {carbon dioxide ($CO_2$) + 1,1-difluoroethene (R1132a)} at temperatures from 220 K to 350 K

**Davide MENEGAZZO*[(a,b)], Aaron J. ROWANE[(c)], Laura FEDELE[(a)], Sergio BOBBO[(a)], Giulia LOMBARDO[(a,b)], Mark O. McLINDEN[(c)]**

[(a)]Istituto per le Tecnologie della Costruzione, Consiglio Nazionale delle Ricerche, Corso Stati Uniti 4, 35127 Padova, Italy

[(b)]Dipartimento di Ingegneria Industrial-Sezione Fisica Tecnica, Università degli Studi di Padova, Via Venezia 1, 35131 Padova, Italy

[(c)] Applied Chemicals and Materials Division, National Institute of Standards and Technology, 325 Broadway, Boulder, CO 80305, USA

*Corresponding author: davide.menegazzo@phd.unipd.it

## ABSTRACT

The blend of carbon dioxide and R1132a has been suggested as a feasible alternative to R23 in low-temperature devices. In this work, we present new experimental data for compressed-liquid density, vapour density and compressed-liquid speed of sound for the binary system $CO_2$ + R1132a by means of a two-sinker densimeter and a pulse-echo-type instrument, respectively. The measurements cover the temperature range of 220 K to 350 K with pressures to 30 MPa for density; the speed of sound measurements cover the range 230 K to 350 K with pressures to 55 MPa; for both properties two mixture compositions were measured. Finally, we present an Equation of State (EoS) correlation for the experimental data based on a Helmholtz free energy model, which shows a good agreement with the measurements. The mixture strongly absorbed the sound pulse, and the usual dual-path analysis was not possible; thus, we developed a method using only the short-path signal.

Keywords: Refrigeration, Carbon Dioxide, HFO, Density, Speed of Sound

## 1. INTRODUCTION

In recent years, an important effort has been spent in the research for innovative refrigerants with environmental impacts lower than currently used fluids. Such impacts are expressed in terms of global warming potential (GWP) and ozone depletion potential (ODP). International regulations and agreements, such as the F-gas Regulation of the European Union (2014) and Kigali Amendment to the Montreal Protocol (2016), have the goal to gradually phase down the production and consumption of the hydrofluorocarbon (HFC) based refrigerants in most HVAC&R applications. To date, McLinden et al. (2017, 2020) identified a limited number of low-GWP refrigerants, mostly hydrofluoroolefins (HFOs) and hydrochlorofluoroolefins (HCFOs), as feasible alternatives for the refrigerants used in the most common air-conditioning applications based on chemical, safety, environmental and thermodynamic criteria.

Ultra-low temperature (ULT) refrigerating systems are not currently restricted by the main regulations (Mota-Babiloni et al., 2020). For ULT applications, R23 and R508 are commonly used (Mota-Babiloni et al., 2020), but they are characterized by high-GWP values: 14800 and 13400 respectively (Solomon et al., 2007). $CO_2$ is considered an interesting solution for low temperature application, being non-flammable, chemically stable and inexpensive (Barta et al., 2021). At the same time, the triple point of 216.59 K limits the usage of carbon dioxide for ULT applications. Therefore, mixing $CO_2$ with refrigerants that would lower the triple point of the mixture offers an interesting solution to this issue (Di Nicola et al., 2013). Among HFO and HCFO refrigerants,

1,1-difluoroethene (R1132a) is one of the few suitable working fluids for ULT applications (Mota-Babiloni et al., 2020), and Tomassetti et al. (2022), showed that a blend of 75% $CO_2$ and 25% R1132a has a triple point of 203 K.. R1132a is flammable and potentially susceptible to stability issues if used with certain materials. Blending R1132a with an inert fluid, such as $CO_2$, will reduce its flammability and potentially improve its stability (although we did not investigate either of these in the present work).

Despite the potential promise of this mixture, only one set of data was available and obtained through private communication with the research team of Università Politecnica delle Marche, who measured the vapour density of the blend. Thus, the present work aims to compensate for this lack of information with new measurements on the compressed-liquid density, vapour density and the compressed-liquid speed of sound of the system $CO_2$/R1132a by means of a two-sinker densimeter (McLinden and Splett, 2008; McLinden, 2009) and a pulse-echo-type instrument (McLinden and Perkins, 2023), respectively. The measurements have been performed over the temperature range of 220 K to 350 K with pressures to 30 MPa for density, and a range of 230 K to 350 K with pressures to 55 MPa for speed of sound. The analysis of the vapour density results also allowed estimation of the dew point pressures corresponding to the measured temperatures. For both experiments two mixture compositions were measured. Finally, we present an Equation of State (EoS) correlation for the experimental data based on a Helmholtz energy model, showing a good agreement with the measurements of compressed-liquid density for the binary systems, while some concerns are highlighted in the prediction of speed of sound.

## 2. EXPERIMENTAL SECTION

### 2.1. Materials and sample preparation

Table 1 specifies the materials used in this work. The $CO_2$ sample was used as provided, without further purification. The R1132a sample was degassed by freezing/pumping/thawing. We gravimetrically prepared vapour phase samples as explained in Richter and McLinden (2014), with the weighings based on the double-substitution procedure of Harris and Torres (2003). Table 2 lists the two compositions studied for the binary mixtures. The same samples were measured, first, on the 2-sinker densimeter and then on the speed of sound apparatus.

**Table 1. Material specification.**

| Chemical name | CAS Number | Source | Purity [molar fraction] |
|---|---|---|---|
| carbon dioxide ($CO_2$) | 124-38-9 | Scott | 0.99997 |
| 1,1-difluoroethene (R1132a) | 75-38-7 | Koura | 0.9995 |
| propane | 74-98-6 | Scott | 0.99999 |

**Table 2. Mixture compositions.**

| | Composition (molar basis) | Composition (mass basis) | Molar mass [g/mol] |
|---|---|---|---|
| Mix 1 | 0.5942/0.4058 | 0.5016/0.4984 | 52.137 |
| Mix 2 | 0.7926/0.2074 | 0.7242/0.2758 | 48.165 |

### 2.2. Compressed liquid and superheated vapour density measurements

We measured the density of the binary $CO_2$/R1132a mixtures by means of a 2-sinker densimeter. The experiment has already been described in previous works (McLinden and Splett, 2008; McLinden, 2009; McLinden and Lösch-Will, 2007). Briefly, this instrument uses the Archimedes principle to provide the absolute density of sample at a specified temperature and pressure by a differential method: two sinkers, one made of titanium and one of tantalum, with the same mass but different volumes are immersed in the sample and weighed, one at time, through a magnetic suspension coupling. The basic working equation is

$$\rho_{\text{fluid}} = \left[(m_1 - m_2) - \frac{(W_1 - W_2)}{\alpha\phi}\right] / (V_1 - V_2) \qquad \text{Eq. (1)}$$

where $m_i$ are the sinker masses, $W_i$ are the balance readings, $V_i$ are the sinker volumes, for the $i$-th sinker. The terms $\alpha$ and $\phi$ are correction factors which account for the balance calibration and the force-transmission error respectively, as described by McLinden and Richter (2016). A standard platinum resistance thermometer (SPRT) located in a thermowell on the measuring cell measured the temperature; it was calibrated on ITS-90 by using fixed-point cells in the temperature range from 83 to 505 K. One of three vibrating-quartz-crystal-type transducers (full-scale pressure ranges of 2.75 MPa, 14 MPa and 69 MPa) were calibrated by means of a piston gauge and used to measure the pressure in the cell. The experimental uncertainty of such experiment is reported in detail in previous work (McLinden and Lösch-Will, 2007). Considering a coverage factor $k = 2$, the expanded uncertainty in density is

$$U_c(\rho) = \{(52)^2 + [0.75 \cdot T \cdot 293]^2 + (1.25 \cdot p)^2\}^{0.5} \cdot 10^{-6} \cdot \rho + 0.0014 \qquad \text{Eq. (2)}$$

where $T, p$ and $\rho$ are expressed in K, MPa and kg/m$^3$ respectively. Eq. 2 accounts for the standard uncertainties in weighings, sinker volumes, and the force transmission error.

Estimation of the dew point pressures

As described by McLinden and Richter (2016), Eq. 1 is based on the assumption that all the quantities involved in the calculation of the density were constant over the measurement time of one point, which was about 12 minutes. Moreover, the sinker masses were assumed to be constant and equal to the values determined prior to their installation in the densimeter. These assumptions apply if the sample was in a homogenous liquid or vapour state. But near the saturation line, sample can adsorb onto the surfaces of the sinkers, thus changing their effective masses. In the 2-phase region there can be bulk condensation of sample onto the sinkers. These effects will result in a change in the calculated value of the coupling factor $\phi$. (The difference $(\phi - 1)$ indicates the magnitude of the force-transmission error.) As shown in Fig. 1, $(\phi - 1)$ drastically increased when the sample was in 2-phase. This allowed to estimate the dew point pressure by extrapolating the lines which represent the vapour phase (orange line) and the 2-phase region (green line).

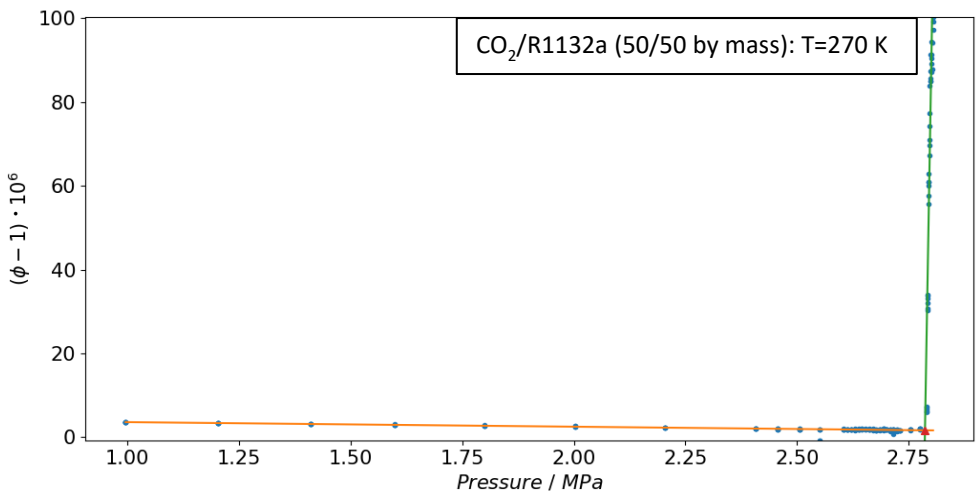


**Figure 1. Dew point pressure estimation; blue dots: experimental data; orange line: vapour data regression line; green line: 2-phase data regression line; red triangle: dew point pressure.**

### 2.3. Compressed liquid speed of sound measurements

To measure the speed of sound of the mixture, we used the pulse-echo-type instrument described by McLinden and Perkins (2023). Briefly, a quartz crystal immersed in the liquid sample was used as the ultrasonic signal transmitter and receiver. The crystal was placed between two sets of tubular spacers and

reflectors. The spacers were approximately 12 mm and 30 mm long; they defined the "short" and the "long" echo paths, respectively. When in the signal-transmitting mode, an arbitrary function generator excited the crystal with a 10-cycle sinusoidal voltage at the crystal's resonant frequency of 8.00 MHz. The generated tone burst was emitted from both faces of the crystal and traversed the fluid along the short and long paths and then returned from the reflectors. The crystal transducer received the echoes, which it converted to electrical signals, which then passed through a three-stage amplifier before being recorded using a digital storage oscilloscope. The oscilloscope stored the data as 16-bit data ranging from 0 to 65535, with a value of 32768 corresponding to zero volts. The measurement cell was installed in a type 316 stainless-steel pressure vessel and immersed in a liquid thermostated bath providing temperature control. The temperature was measured by means of a SPRT placed adjacent to the cell.

### 2.3.1. Dual-path analysis for speed of sound

The echoes recorded by the instrument were then analysed offline to compute the speed of sound:

$$w = \frac{2 * (L_{\text{long}} - L_{\text{short}})}{\Delta\tau} \qquad \text{Eq. (3)}$$

where $L_{\text{long}}$ and $L_{\text{short}}$ are the long-path and the short-path, respectively; $\Delta\tau$ is the time interval between the short and the long-path echo arrivals. The difference between $L_{\text{long}}$ and $L_{\text{short}}$ is dependent on temperature and pressure, and this was based on a calibration with propane. The time difference $\Delta\tau$ is determined with the method described in McLinden and Perkins (2023) based on the superposition of the long- and short-path echoes.

As done in McLinden and Perkins (2023) and Rowane et al. (2022a), we measured the speed of sound of propane along an isochore ($T$ = 230 K to 350 K; $p$ = 1 MPa to 62 MPa) and calculated the difference ($L_{\text{long}} - L_{\text{short}}$) by inverting Eq. 3 and taking the speed of sound of propane as known value, calculated with the EoS of Lemmon et al. (2009). Then, we compared it with the same analysis obtained from the calibration made in November 2019. Fig. 2 shows the results of the comparison, which confirm that after three years the calibration performed in 2019 remained stable.

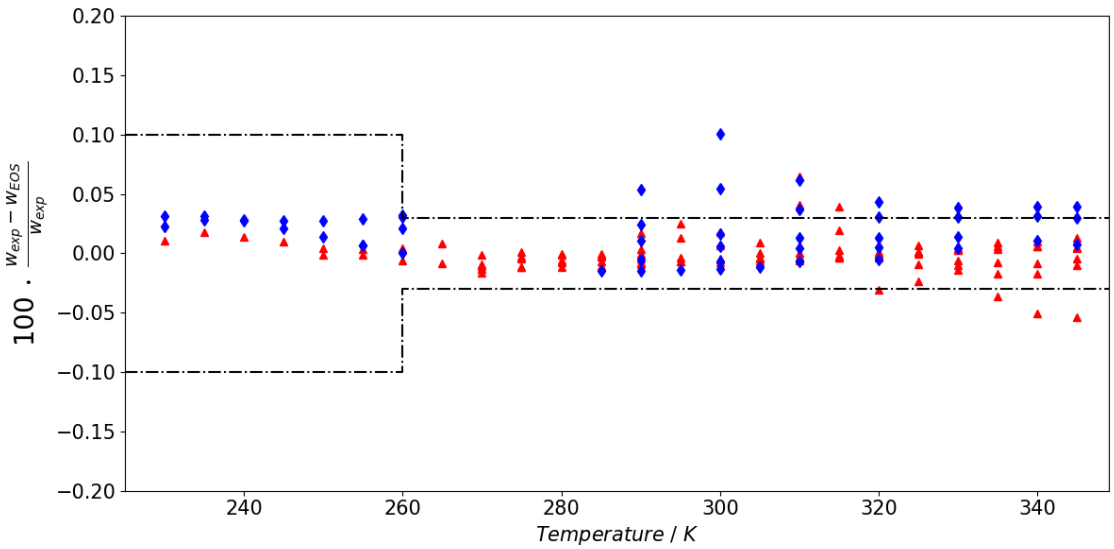


**Figure 2. Comparison of measured propane speed of sound data, $w_{exp}$, from 2019 (red triangles) and from 2022 (blue diamonds) measurements with the EOS of Lemmon et al. (2009), $w_{EOS}$. The dashed lines represent the estimated uncertainty for the EOS.**

The combined expanded uncertainty in the speed of sound was estimated by:

$$\frac{U_c(w)}{m \cdot s^{-1}} = \sqrt{\left\{u^2(w) + \left[\frac{\partial w}{\partial T}\right]^2 u^2(T) + \left[\frac{\partial w}{\partial p}\right]^2 u^2(p) + \left[\frac{\partial w}{\partial x_i}\right]^2 u^2(x_i)\right\}} \qquad \text{Eq. (4)}$$

The major uncertainty sources $u$ in the speed of sound were due to the path length calibration with propane and the weaker signal magnitude as the fluid approached the critical point.

### 2.3.2. Single-path analysis for speed of sound

The dual-path analysis requires two clear signals as outputs from the experiment, one for the short-path and one for the long-path. When dealing with fluids characterized by a high sound-absorption, it may occur that the long-path signal is too weak to be distinguished from noise, and even the short-path echo may be very weak. In this case, the dual-pulse analysis method cannot be applied. Fig. 3 compares a low sound-absorption fluid, such as propane, with the mixture we measured in this work, consisting of two components, each of which has high sound-absorption (Lin and Trusler, 2014; Rowane and Perkins, 2023). Such strong sound-absorption can be the result of dispersion, whereby the internal vibrations of the molecule do not damp down before the next sound pulse arrives (El Hawary et al., 2020).

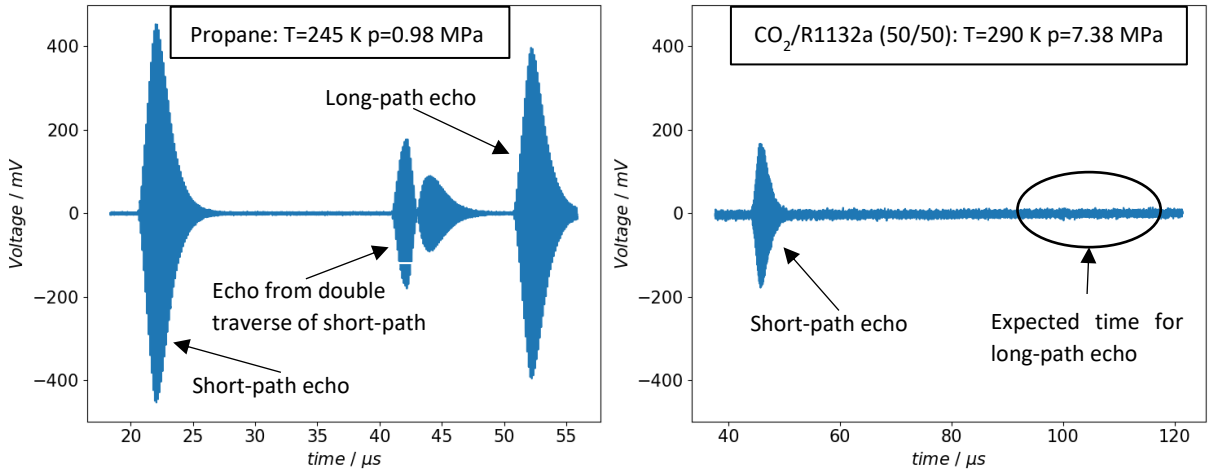


**Figure 3. Comparison between (left) low sound-absorption fluid (propane) and (right) high sound-absorption fluid ($CO_2$/R1132a, 50/50 by mass) – the resolution is not sufficient to show the individual sinusoids (see Fig. 4).**

In this work, we present a new method to obtain a speed of sound value from a very weak signal fluid, based on the analyses of only the short-path echo. With this approach, Eq. 3 is modified as follows:

$$w = \frac{2\, L_{short}}{\tau_1 - \tau_0} \qquad \text{Eq. (5)}$$

where $\tau_0$ represents the moment when the crystal first triggers the pulse and $\tau_1$ the moment in which the crystal starts to receive the short path echo. In the experiment we performed, $\tau_0$ was a fixed delay of 60 ns due to a delay of the function generator between the trigger signal and the start of the pulse signal. Determining $\tau_1$ is the crucial point of this method and the process is graphically explained in Fig. 4. First, through Fast Fourier Transform (FFT) analyses, we apply a low-pass filter to the short-path echo with a cut-off frequency of 8.5 MHz to polish the signal. Then, we calculate the waveform envelope function $f$ comprising the maxima of the sinusoids (orange line in Fig. 4). Finally, we numerically derive the envelope function by means of finite differences considering as abscissa only the time values of the upper peaks, obtaining a vector $f'$: $\tau_1$ is determined as the first time value where $f'$ is higher than an empirical value $\alpha$, called the discriminant. Such value is set depending on the fluid itself and on the noise magnitude. For all the fluids we analysed, $\alpha$ was set at (32768 + 500) in the 16-bit scale ranging from 0 to 65535.

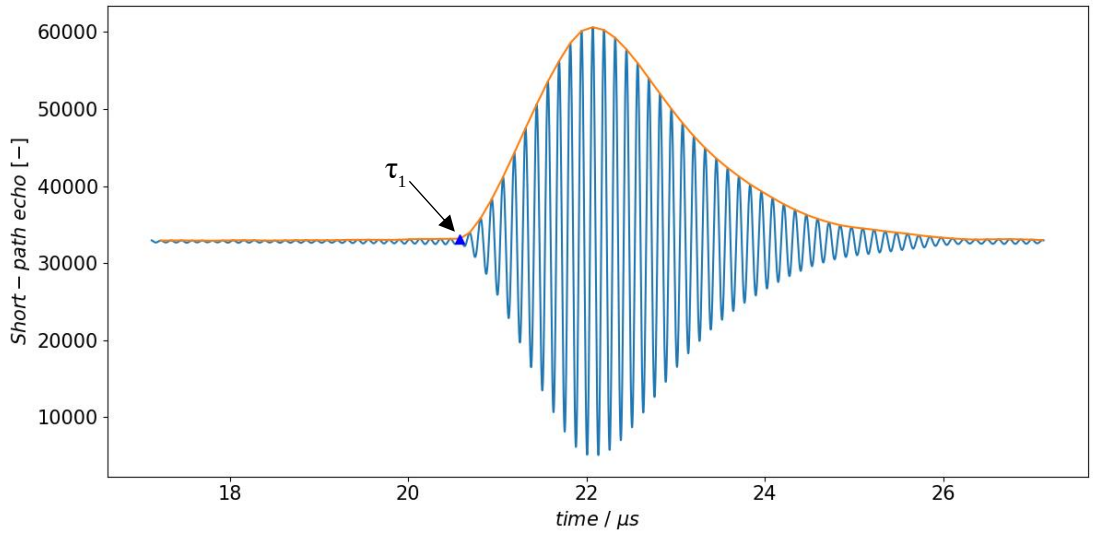


**Figure 4. 1-pulse analyses of a short-path signal; blue line: short-path echo; orange line: upper peaks envelope function; blue triangle: $\tau_1$ determined by this method. On the y-scale are reported the voltage values converted to 16-bits (see section 2.3).**

To validate the new approach, we compared the results obtained with a dual-path analysis on the propane data acquired for the validation of the instrument, which resulted in strong echo signals, with the same data analysed with the single-path approach. As shown in Fig. 5, the systematic bias of ~0.6% indicates that the two methods are in reasonable agreement. We performed the analyses with Python code; in particular, we used the scipy package (Virtanen et al., 2020) for the signal analysis.

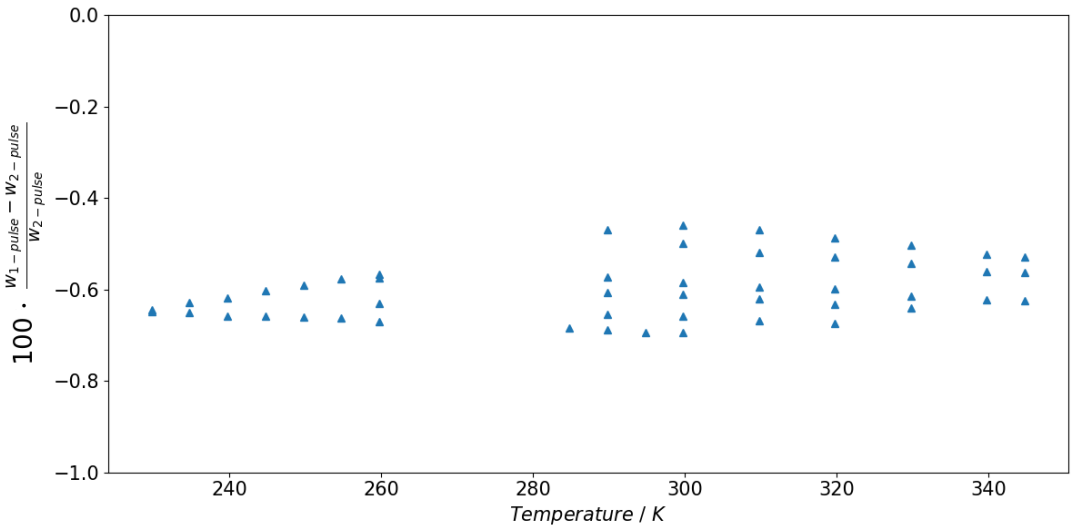


**Figure 5. Comparison between dual-pulse-echo method and single-pulse-echo method on propane speed of sound validation data.**

The major sources of uncertainty in the single-pulse method are related to the short-path length and the determination of $\tau_1$. This is because the object of the calibration with propane was the difference between short-path and long-path length, instead of the short-path length itself. Moreover, $\tau_1$ is determined through an extrapolation of the signal waveform envelope; this extrapolation depends on the selected value for the discriminant. Considering the aforementioned and the relative difference of ~0.6% obtained for the propane, we conservatively estimate an expanded ($k$ = 2) uncertainty of 1% for the single-path method. While this is considerably higher than the 0.05% uncertainty typically obtained for the dual-path method (McLinden and Perkins, 2023; Rowane et al., 2022), the data are nonetheless very valuable for fitting a mixture model.

## 3. RESULTS

### 3.1. Density

Tables 3 and 4 present vapour- and liquid-phase density data for the first composition; Tables 5 and 6 present the same for the second composition. The relative combined uncertainty of the vapour and liquid phase densities ranged from (0.031 – 0.085)% and (0.030 – 0.132)%. Standard uncertainties in the pressure were less than 0.011 kPa and 1.879 kPa for vapour and liquid phase measurements, respectively. The uncertainty in the temperature was 3 mK. Table 7 presents the estimation of the dew point pressures at temperatures of 240 K, 255 K and 270 K.

**Table 3. Experimental vapour-phase density (p, ρ, T) data for $CO_2$/R1132a (Mix 1)**

| *T*/K | *p*/MPa | *ρ*/kg·m$^{-3}$ | *T*/K | *p*/MPa | *ρ*/kg·m$^{-3}$ | *T*/K | *p*/MPa | *ρ*/kg·m$^{-3}$ |
|---|---|---|---|---|---|---|---|---|
| 270.005 | 0.99739 | 25.4812 | 255.017 | 0.48890 | 12.7064 | 239.995 | 0.39286 | 10.8372 |
| 270.005 | 1.20449 | 31.4737 | 255.014 | 0.65551 | 17.3762 | 239.998 | 0.40683 | 11.2450 |
| 270.005 | 1.41155 | 37.7815 | 255.013 | 0.81447 | 22.0223 | 240.001 | 0.50112 | 14.0414 |
| 270.006 | 1.60105 | 43.8728 | 255.013 | 0.96043 | 26.4733 | 239.999 | 0.60337 | 17.1688 |
| 270.005 | 1.80235 | 50.7321 | 255.012 | 1.11399 | 31.3720 | 239.999 | 0.69994 | 20.2217 |
| 270.005 | 2.00560 | 58.1370 | 255.013 | 1.25649 | 36.1426 | 240.001 | 0.80246 | 23.5790 |
| 269.998 | 2.20514 | 65.9763 | 255.014 | 1.40342 | 41.3222 | 239.999 | 0.90909 | 27.2129 |
| 270.004 | 2.40939 | 74.7268 | 255.012 | 1.55174 | 46.8646 | 239.998 | 1.01099 | 30.7688 |
| 270.006 | 2.45843 | 76.9523 | | | | | | |
| 270.005 | 2.50756 | 79.1583 | | | | | | |

**Table 4. Experimental liquid-phase density (p, ρ, T) data for CO2/R1132a (Mix 1)**

| *T*/K | *p*/MPa | *ρ*/kg·m$^{-3}$ | *T*/K | *p*/MPa | *ρ*/kg·m$^{-3}$ | *T*/K | *p*/MPa | *ρ*/kg·m$^{-3}$ |
|---|---|---|---|---|---|---|---|---|
| 260.009 | 11.53043 | 976.6414 | 284.998 | 7.59705 | 830.8582 | 319.992 | 8.08113 | 370.3310 |
| 260.009 | 10.15914 | 970.2409 | 284.998 | 6.60926 | 817.3527 | 325.003 | 8.60623 | 368.0478 |
| 260.010 | 8.07897 | 959.7303 | 284.999 | 5.16243 | 792.3559 | 330.001 | 9.12698 | 366.4853 |
| 260.010 | 6.09538 | 948.6340 | 290.000 | 6.84515 | 783.9410 | 334.998 | 9.64491 | 365.2865 |
| 260.010 | 4.46759 | 938.4970 | 295.002 | 8.31166 | 772.6632 | 339.997 | 10.16030 | 364.3370 |
| 260.010 | 3.34620 | 930.8261 | 304.997 | 11.91402 | 765.3078 | 344.994 | 10.67164 | 363.4607 |
| 270.005 | 7.48879 | 911.5078 | 309.994 | 13.79790 | 763.4581 | 349.993 | 11.18081 | 362.7219 |
| 275.018 | 9.48732 | 902.2674 | 314.999 | 15.69843 | 761.9432 | 349.989 | 9.03499 | 256.1346 |
| 279.997 | 12.13380 | 898.4532 | 319.996 | 17.60451 | 760.7189 | 349.993 | 7.02977 | 175.0538 |
| 284.997 | 14.93925 | 896.0024 | 319.993 | 14.10902 | 707.7691 | 349.994 | 4.95675 | 109.9060 |
| 284.998 | 12.94505 | 881.9747 | 319.995 | 12.10088 | 660.8096 | 349.995 | 3.11655 | 63.3231 |
| 284.998 | 10.23493 | 859.3568 | 319.995 | 10.32228 | 591.8146 | 349.994 | 1.48009 | 28.1097 |
| 284.998 | 8.61987 | 842.9441 | | | | | | |

**Table 5. Experimental vapour-phase density (p, ρ, T) data for CO2/R1132a (Mix 2)**

| *T*/K | *p*/MPa | *ρ*/kg·m$^{-3}$ | *T*/K | *p*/MPa | *ρ*/kg·m$^{-3}$ | *T*/K | *p*/MPa | *ρ*/kg·m$^{-3}$ |
|---|---|---|---|---|---|---|---|---|
| 270.005 | 0.91468 | 21.2169 | 255.015 | 0.71310 | 17.4092 | 240.005 | 0.57084 | 14.7960 |
| 270.005 | 1.20097 | 28.5893 | 255.014 | 0.90137 | 22.4803 | 240.005 | 0.65940 | 17.3022 |
| 270.004 | 1.53242 | 37.7549 | 255.015 | 1.15607 | 29.7439 | 240.004 | 0.74403 | 19.7596 |
| 270.004 | 1.81566 | 46.1987 | 255.016 | 1.30884 | 34.3593 | 240.004 | 0.82426 | 22.1512 |
| 270.004 | 2.11555 | 55.9004 | 255.013 | 1.51562 | 40.9755 | 240.004 | 0.90173 | 24.5222 |
| 270.005 | 2.41137 | 66.4467 | 255.014 | 1.69858 | 47.2452 | 240.004 | 1.04638 | 29.1287 |
| 270.005 | 2.72228 | 78.9361 | 240.006 | 0.28053 | 7.0076 | 240.004 | 1.11455 | 31.3055 |
| 255.017 | 0.50768 | 12.1268 | 240.005 | 0.47835 | 12.2478 | | | |

**Table 6. Experimental liquid-phase density (p, ρ, T) data for CO2/R1132a (Mix 2)**

| *T*/K | *p*/MPa | *ρ*/kg·m$^{-3}$ | *T*/K | *p*/MPa | *ρ*/kg·m$^{-3}$ | *T*/K | *p*/MPa | *ρ*/kg·m$^{-3}$ |
|---|---|---|---|---|---|---|---|---|
| 220.009 | 3.13725 | 1123.538 | 275.022 | 12.70560 | 944.668 | 314.998 | 21.18189 | 824.733 |
| 220.009 | 2.28979 | 1121.435 | 275.021 | 10.10741 | 928.557 | 314.998 | 18.10082 | 794.454 |
| 230.007 | 7.94735 | 1101.056 | 275.021 | 7.58372 | 910.072 | 314.998 | 15.14795 | 755.779 |
| 240.000 | 14.52478 | 1084.635 | 280.006 | 9.37734 | 897.649 | 314.998 | 12.15686 | 695.197 |
| 249.998 | 24.64247 | 1079.209 | 284.999 | 11.98351 | 892.598 | 314.998 | 9.56178 | 575.384 |
| 250.000 | 20.00265 | 1066.759 | 290.002 | 14.81469 | 889.715 | 320.004 | 10.64327 | 572.815 |
| 250.001 | 16.11627 | 1055.314 | 295.001 | 17.68874 | 887.470 | 330.002 | 12.82950 | 569.792 |
| 250.000 | 12.27400 | 1042.854 | 304.998 | 23.53176 | 884.249 | 340.003 | 15.02912 | 567.700 |
| 250.001 | 9.29265 | 1032.187 | 309.998 | 26.45046 | 882.855 | 350.001 | 17.23002 | 566.022 |
| 250.002 | 7.14161 | 1023.826 | 315.000 | 29.36038 | 881.550 | 350.002 | 15.02601 | 492.875 |
| 260.010 | 11.90923 | 1003.427 | 314.998 | 24.76459 | 852.682 | 350.002 | 13.19707 | 413.577 |
| 270.004 | 19.71506 | 997.490 | 314.998 | 21.18189 | 824.733 | 350.001 | 9.17858 | 229.483 |
| 275.020 | 23.76517 | 995.448 | 314.998 | 18.10082 | 794.454 | 350.001 | 6.01942 | 126.459 |
| 275.020 | 20.46370 | 982.394 | 314.998 | 15.14795 | 755.779 | 350.002 | 3.79986 | 72.277 |
| 275.019 | 17.62069 | 969.936 | 314.998 | 12.15686 | 695.197 | 350.000 | 2.03840 | 36.230 |
| 275.021 | 15.19976 | 958.178 | 314.998 | 24.76459 | 852.682 | | | |

**Table 7. Estimation of the dew points pressures for the two compositions of the binary mixture $CO_2$/R1132a.**

| **Mix 1** | | **Mix 2** | |
|---|---|---|---|
| T/K | p/MPa | T/K | p/MPa |
| 270.01 | 2.789 | 270.01 | 3.039 |
| 255.01 | 1.827 | 255.01 | 2.002 |
| 240.00 | 1.138 | 240.00 | 1.240 |

### 3.2. Speed of sound – results

Tables 8 and 9 present the data for the first and second composition, respectively. For each point, the calculation method can be inferred from the uncertainty in sound speed: $U(w)$ = 1.0 % corresponds to the single-path method (see Section 2.3.2); the dual-path method was used for all other points. The standard uncertainty in the temperature is 3 mK.

**Table 8. Experimental compressed liquid data for CO2/R1132a (Mix 1).**

| *T*/K | *p*/MPa | *w*/m·s$^{-1}$ | *U(w)*/% | *T*/K | *p*/MPa | *w*/m·s$^{-1}$ | *U(w)*/% |
|---|---|---|---|---|---|---|---|
| 245.007 | 6.5643 | 700.149 | 0.031 | 264.993 | 5.2828 | 542.681 | 1.0 |
| 250.003 | 9.7048 | 698.728 | 0.031 | 269.991 | 5.7847 | 511.047 | 1.0 |
| 254.995 | 13.3984 | 705.278 | 0.031 | 274.995 | 7.6880 | 506.459 | 1.0 |
| 274.996 | 28.9865 | 735.030 | 0.031 | 279.999 | 10.2733 | 514.706 | 1.0 |
| 280.001 | 32.9214 | 742.633 | 0.031 | 285.002 | 12.9555 | 523.912 | 1.0 |
| 285.003 | 36.8426 | 750.089 | 0.031 | 290.003 | 15.6679 | 533.910 | 1.0 |
| 290.005 | 40.7443 | 757.359 | 0.031 | 294.999 | 18.3884 | 543.521 | 1.0 |
| 264.997 | 9.8414 | 606.174 | 1.0 | 300.000 | 21.1088 | 552.250 | 1.0 |
| 269.994 | 12.8032 | 611.293 | 1.0 | 304.998 | 23.8199 | 560.507 | 1.0 |
| 290.005 | 24.1150 | 627.939 | 1.0 | 309.999 | 26.5210 | 568.222 | 1.0 |
| 295.000 | 26.8204 | 631.556 | 1.0 | 314.993 | 29.1977 | 575.768 | 1.0 |
| 310.000 | 33.7716 | 635.156 | 0.031 | 320.002 | 31.8625 | 584.956 | 1.0 |
| 314.993 | 36.1435 | 638.097 | 0.031 | 325.007 | 34.4963 | 589.815 | 1.0 |
| 320.002 | 38.4192 | 638.887 | 0.031 | 329.999 | 37.0807 | 596.345 | 1.0 |
| 325.007 | 40.6006 | 640.137 | 0.031 | 335.000 | 39.5675 | 602.761 | 1.0 |
| 320.0029 | 33.1061 | 594.452 | 1.0 | 340.004 | 40.6139 | 598.227 | 1.0 |
| 320.001 | 32.9898 | 595.052 | 1.0 | | | | |

**Table 9. Experimental compressed liquid data for CO2/R1132a (Mix 2).**

| *T*/K | *p*/MPa | *w*/m·s$^{-1}$ | *U(w)*/% | *T*/K | *p*/MPa | *w*/m·s$^{-1}$ | *U(w)*/% |
|---|---|---|---|---|---|---|---|
| 235.008 | 5.0150 | 798.153 | 0.043 | 314.994 | 60.6660 | 810.000 | 0.037 |
| 240.001 | 5.6285 | 769.252 | 0.045 | 320.003 | 64.7302 | 816.801 | 0.037 |
| 250.005 | 7.1567 | 712.682 | 0.051 | 254.9937 | 6.3951 | 671.104 | 1.0 |
| 254.995 | 10.6277 | 713.350 | 1.0 | 259.9873 | 9.7499 | 673.737 | 1.0 |
| 259.990 | 14.6892 | 722.549 | 1.0 | 264.9968 | 13.5301 | 680.286 | 1.0 |
| 280.003 | 31.5783 | 754.059 | 1.0 | 285.0032 | 29.2277 | 715.990 | 1.0 |
| 285.004 | 35.8073 | 764.569 | 1.0 | 290.0055 | 33.1539 | 724.635 | 1.0 |
| 290.006 | 40.0131 | 772.551 | 0.041 | 295.0007 | 37.0579 | 730.791 | 1.0 |
| 295.002 | 44.1868 | 780.976 | 0.040 | 300.0015 | 40.9454 | 740.495 | 1.0 |
| 300.002 | 48.3503 | 788.566 | 0.039 | 310.0005 | 48.2200 | 751.321 | 1.0 |
| 304.999 | 52.4805 | 795.898 | 0.039 | 314.9936 | 52.0279 | 760.142 | 1.0 |
| 310.000 | 56.5904 | 803.053 | 0.038 | 320.003 | 55.8166 | 767.927 | 0.039 |

## 4. MODELLING

### 4.1. Helmholtz energy model

We applied a parametric multi-fluid model based on the Helmholtz-energy-explicit formulation to model the behaviour of the $CO_2$/R1132a blend. Previous papers (Bell, 2022; Bell et al., 2022) described the method in detail; briefly the Helmholtz energy, $a$, is defined as:

$$\alpha(\tau,\delta,z) = \frac{a}{RT} = \alpha^{ig} + \alpha^{r} = \alpha^{ig} + \alpha^{r}_{CS} + \alpha^{r}_{\mathrm{dep}} \qquad \text{Eq. (6)}$$

Where $\alpha$ is expressed as the sum of the ideal contribution, $\alpha^{ig}$, and the residual contribution, $\alpha^{r}$, of Helmholtz energy. The residual contribution is then split in a corresponding-state contribution, $\alpha^{r}_{CS}$ (Eq. 7), and a departure function contribution (Eq. 11).

$$\alpha_{CS}^{r} = \sum_{i=1}^{N_{\text{components}}} z_i \alpha_{0,i}^{r}(\tau, \delta) \qquad \text{Eq. (7)}$$

The reduced variables $\tau$ and $\delta$ are defined as $\tau = T_{red}(\boldsymbol{z})/T$ and $\rho = \rho/\rho_{red}(\boldsymbol{z})$, with $\boldsymbol{z}$ as vector containing the molar fraction of each component. The subscript 0 in Eq. 7 refers to the *i*-th pure fluid. The reducing functions $T_{red}$ and $\rho_{red}$ are given by:

$$Y_{\text{red}}(\boldsymbol{z}) = \sum_{i=1}^{N} z_i^2 Y_{crit,i} + \sum_{i=1}^{N} \sum_{j=i+1}^{N} 2 z_i z_j \frac{z_i + z_j}{\beta_{Y,ij}^2 z_i + z_j} Y_{i,j} \qquad \text{Eq. (8)}$$

Where $Y$ is the parameter of interest (either the molar volume $v = 1/\rho$ or the temperature $T$). Then, $T_{i,j}$ and $\rho_{i,j}$ are given by:

$$T_{ij} = \beta_{T,ij} \gamma_{T,ij} \frac{x_i + x_j}{\beta_{T,ij}^2 x_i + x_j} (T_{c,i} T_{c,j})^{1/2} \qquad \text{Eq. (9)}$$

$$\frac{1}{\rho_{ij}} = \beta_{v,ij} \gamma_{v,ij} \frac{x_i + x_j}{\beta_{v,ij}^2 x_i + x_j} \frac{1}{8} \left( \frac{1}{{\rho_{c,i}}^{1/3}} + \frac{1}{{\rho_{c,j}}^{1/3}} \right)^3 \qquad \text{Eq. (10)}$$

The departure function in Eq. (6) is given by:

$$\alpha_{\text{dep}}^{r} = \sum_{i=1}^{N} \sum_{j=i+1}^{N} z_i z_j F_{ij}\, \alpha_{ij}^{r}(\tau, \delta) \qquad \text{Eq. (11)}$$

Where the departure term $\alpha_{ij}^{r}$ is an arbitrary function of $(\tau, \delta)$.

With this model, all the thermodynamic properties of a mixture can be expressed as function of the reduced temperature, $\tau$, reduced density, $\delta$, and composition $\boldsymbol{z}$ through the definition of the Helmholtz energy, $a$, and its derivative, as detailed by Lemmon et al. (2009).

### 4.2. Correlation

In this work, we fitted the binary interaction parameters and the departure function of Eq. 12 by means of an Adaptive Search Development – Particle Swarm Optimization (ASD-PSO) algorithm (Ardizzon et al., 2015).

$$\alpha_{ij}^{r}(\tau, \delta) = \sum_{k} n_k \tau^{t_k} \delta^{d_k} e^{-\eta_k(\delta - \epsilon_k) - \beta_k(\tau - \gamma_k)} \qquad \text{Eq. (12)}$$

Where *k* is the number of terms in the summation, $n_k, t_k, d_k, \eta_k, \epsilon_k, \beta_k$ and $\gamma_k$ are the parameters to optimize for each departure function. The objective function to minimize is shown in Eq. 13.

$$F_{obj} = \sqrt{\frac{1}{N} \sum_{i} res_{\rho}^2} + \sqrt{\frac{1}{N} \sum_{i} \left( \frac{w_{exp,i} - w_{calc,i}}{w_{exp,i}} \right)^2} \qquad \text{Eq. (13)}$$

Where $res_{\rho}$ is the residual relative error of the *i*-th density data point, calculated as in Bell (2022).

The accuracy of a thermodynamic model depends on both the departure function and the EoS of the pure fluids. In this work, only the departure function has been regressed. We adopted the model of Span and Wagner (1996) for pure $CO_2$ and the EoS proposed by Low (2018) for R1132a. While $CO_2$ is a well-characterized fluid, the same is not the case for R1132a. Rowane and Perkins (2023) highlighted the limitations of the available EoS for R1132a in the calculation of the speed of sound; they found an average error in the speed of sound for the pure R1132a of 6.4%. Considering this, we fitted the mixture model

including only the density data (including the data obtained through private communication) applying the aforementioned ASD-PSO algorithm; thus, we neglected the speed of sound data in the fitting, but then the model was compared to the speed of sound data. The average model error is 0.3% for density and 3.4% for speed of sound. The model is shown in Table 10.

**Table 10. Fitted mixture model for CO2/R1132a based only on density data.**

| Binary Interaction Parameters | | | |
|---|---|---|---|
| $\beta_T$ | 1.03001 | $\gamma_T$ | 0.97089 |
| $\beta_v$ | 0.97059 | $\gamma_v$ | 0.94482 |
| **Departure function** | | | |
| | $k$=1 | $k$=2 | $k$=3 |
| $\beta_k$ | 1.9749 | 1.8999 | 0.8045 |
| $d_k$ | 1 | 2 | 3 |
| $\epsilon_k$ | 0.0410 | 0.5765 | 0.1102 |
| $\eta_k$ | 0.2839 | 2.1158 | 1.3085 |
| $\gamma_k$ | 1.7059 | 1.8328 | 0.9627 |
| $n_k$ | -0.7879 | 0.1747 | 0.0741 |
| $t_k$ | 1.0098 | 3.5306 | 3.9436 |

## 5. CONCLUSIONS

In this work, we presented experimental measurements on the $CO_2$/R1132a mixture, identified as an interesting low-GWP alternative to R23 for low-temperature refrigeration. We measured 84 points of compressed-liquid density, 49 points of vapour density and 57 points of compressed-liquid speed of sound, across two mixture compositions. Given the high sound-absorption which characterized both the components of the mixture, we introduced a novel technique to analyse cases with very weak signals. This technique is based only on the analysis of the short-path echo with an estimated uncertainty of 1%; it was used when the usual dual-path technique was not applicable because the long-path signal was not detected. The data measured in this work were then used to fit a mixture model through a Helmholtz energy-explicit-type equation of state. In particular, the binary interaction parameters and a Gaussian-type departure function have been regressed based on the available EoS for the pure fluids making up the blend. As already observed in previous work, the available EoS for R1132a is not accurate for the speed of sound calculation and this reflected on the mixture model. Thus, we presented a correlation fitted only to the density data of the mixture which resulted in an average error of 0.3% in density of the blend. For speed of sound data the average error was 3.4%. Although the speed of sound data were not used to fit the present mixture model, they will be valuable in refining the model once a better EoS becomes available for R1132a.

## NOMENCLATURE

| | | | |
|---|---|---|---|
| $p$ | Pressure (kPa) | R | Molar gas constant (8.314472 $J \cdot mol^{-1} \cdot K^{-1}$) |
| T | Temperature (K) | V | Molar volume ($m^3 \cdot mol^{-1}$) |
| $\rho$ | Density ($kg \cdot m^{-3}$) | m | Mass (kg) |
| $w$ | Speed of sound ($m \cdot s^{-1}$) | L | Length (m) |
| $\tau$ | Time (s) | a | Helmholtz energy |

## REFERENCES


Ardizzon, G., Cavazzini, G., Pavesi, G., 2015. Adaptive acceleration coefficients for a new search diversification strategy in particle swarm optimization algorithms. Inf. Sci., Vol. 299, 337–378.

Barta, R.B., Groll, E.A., Ziviani, D., 2021. Review of stationary and transport $CO_2$ refrigeration and air conditioning technologies. Appl. Therm. Eng., Vol. 185.

Bell, I.H., 2023. Mixture Model for Refrigerant Pairs R-32/1234yf, R-32/1234ze(E), R-1234ze(E)/227ea, R-1234yf/152a, and R-125/1234yf. J. Phys. Chem. Ref. Data, Vol. 52, 013101.

Bell, I.H., Deiters, U.K., Leal, A.M.M., 2022. Implementing an Equation of State without Derivatives: teqp. Ind. Eng. Chem. Res., Vol. 61, 6010–6027.

Di Nicola, G., Arteconi, A., Nardini, G., Stryjek, R., 2013. Solid-liquid equilibria measurements of the carbon dioxide+2,3,3,3-tetrafluoroprop-1-ene and carbon dioxide+trans-1,3,3,3-tetrafluoropropene mixtures. Fluid. Phase Equilib., Vol. 354, 54–58.

El Hawary, A., Mirzaev, S.Z., Meier, K., 2020. Speed-of-Sound Measurements in Liquid n-Pentane and Isopentane. J. Chem. Eng. Data, Vol. 65, 1243–1263.

European Parliament and Council of the European Union, 2014. Regulation (EU) No 517/2014 of the European Parliament and of the Council of 16 April 2014 on fluorinated greenhouse gases and repealing Regulation (EC) No 842/2006 Text with EEA relevance. Available: http://data.europa.eu/eli/reg/2014/517/oj.

Harris, G. L., Torres J. A. 2003. Selected Laboratory and Measurement Practices and Procedures to Support Basic Mass Calibrations. NISTIR 6969.

Lemmon, E.W., McLinden, M.O., Wagner, W., 2009. Thermodynamic properties of propane. III. A reference equation of state for temperatures from the melting line to 650 K and pressures up to 1000 MPa. J. Chem. Eng. Data, Vol. 54, 3141–3180.

Lin, C.W., Trusler, J.P.M., 2014. Speed of sound in (carbon dioxide + propane) and derived sound speed of pure carbon dioxide at temperatures between (248 and 373) K and at pressures up to 200 MPa. J. Chem. Eng. Data, Vol. 59, 4099–4109.

Low, R., 2018. Evaluation of potential use of R-1132a as a refrigerant blend component, in: Refrigeration Science and Technology. International Institute of Refrigeration, 504–511.

McLinden M. O., Splett J., 2008. A Liquid Density Standard Over Wide Ranges of Temperature and Pressure Based on Toluene. J. Res. Natl. Inst. Stand. Technol., Vol. 113, 29-67.

McLinden, M.O., 2009. Thermodynamic properties of propane. I. p - ρ - T behavior from (265 to 500) K with pressures to 36 MPa. J. Chem. Eng. Data, Vol. 54, 3181–3191.

McLinden, M.O., Brown, J.S., Brignoli, R., Kazakov, A.F., Domanski, P.A., 2017. Limited options for low-global-warming-potential refrigerants. Nat. Commun., Vol. 8, 14476.

McLinden, M.O., Huber, M.L., 2020. (R)Evolution of Refrigerants. J. Chem. Eng. Data, Vol. 65, 9, 4176–4193.

McLinden, M.O., Kleinrahm, R., Wagner, W., 2007. Force transmission errors in magnetic suspension densimeters, in: Int. J. Thermoph., Vol. 28, 429–448.

McLinden, M.O., Perkins, R.A., 2023. A Dual-Path Pulse-Echo Instrument for Speed of Sound of Liquids and Dense Gases and Measurements on p-Xylene and Four Halogenated-Olefin Refrigerants [R1234yf, R1234ze(E), R1233zd(E), and R1336mzz(Z)]. J. Chem. Thermodynamics. (under review).

McLinden, M.O., Richter, M., 2016. Application of a two-sinker densimeter for phase-equilibrium measurements: A new technique for the detection of dew points and measurements on the (methane + propane) system. J. Chem. Thermod., Vol. 99, 105–115.

Mota-Babiloni, A., Mastani Joybari, M., Navarro-Esbrí, J., Mateu-Royo, C., Barragán-Cervera, Á., Amat-Albuixech, M., Molés, F., 2020. Ultralow-temperature refrigeration systems: Configurations and refrigerants to reduce the environmental impact. Int. J. Ref., Vol. 111, 147-158.

Outcalt, S.L., Rowane, A.J., 2021. Bubble Point Measurements of Mixtures of HFO and HFC Refrigerants. J. Chem. Eng. Data, Vol. 66, 4670–4683.

Richter, M., McLinden, Mark.O., 2014. Vapor-phase (p, ρ, T, x) behavior and virial coefficients for the (methane + propane) system. J. Chem. Eng. Data 59, 4151–4164.

Rowane, A., Perkins, R.A., 2023. Speed of sound measurements of binary mixtures of 1,1-difluoroethylene (R-1132a) + propane and derived speed of sound of pure R-1132a. (Under submission).

Rowane, A.J., Perkins, R.A., 2022. Speed of Sound Measurements of Binary Mixtures of Hydrofluorocarbons [Pentafluoroethane (R-125), 1,1-Difluoroethane (R-152a), or 1,1,1,2,3,3,3-Heptafluoropropane (R-227ea)] with Hydrofluoroolefins [2,3,3,3-Tetrafluoropropene (R-1234yf) or trans-1,3,3,3-Tetrafluoropropene (R-1234ze(E))]. Int J Thermophys., Vol. 43, 127.

Rowane, A.J., Rasmussen, E.G., McLinden, M.O., 2022. Liquid-Phase Speed of Sound and Vapor-Phase Density of Difluoromethane. J. Chem. Eng. Data, Vol. 67, 10, 3022–3032.

Solomon, S., Quin, D., Manning, M., Marquis, M., Averyt, K., Tignor, M.B.M., Miller, H.L.Jr., Chen, Z., 2007. Climate change 2007 : The physical science basis : Contribution of Working Group I to the Fourth Assessment Report of the Intergovernmental Panel on Climate Change. Cambridge University Press.

Span, R., Wagner, W., 1996. A new equation of state for carbon dioxide covering the fluid region from the triple-point temperature to 1100 K at pressures up to 800 MPa. J. Phys. Chem. Ref. Data, Vol. 25, 1509–1596.

United Nations Environment Programme, 2016. The Kigali Amendment to the Montreal Protocol: HFC Phase-down. Available: https://wedocs.unep.org/20.500.11822/26589.

Virtanen, P., Gommers, R., Oliphant, T.E., Haberland, M., Reddy, T., Cournapeau, D., Burovski, E., Peterson, P., et. al., 2020. SciPy 1.0: fundamental algorithms for scientific computing in Python. Nat. Methods, Vol. 17, 261–272.